Effects of Coherence-Based Beamforming on Breast Ultrasound Elastograms

DOI: 10.1109/ULTSYM.2019.8926022

Effects of Coherence-Based Beamforming on Breast Ultrasound Elastograms

Giulia Matrone
Dept. of Electrical, Computer and Biomedical Engineering
University of Pavia
Pavia, Italy
giulia.matrone@unipv.it

Elena Lashkevich
Dept. of Electrical, Computer and Biomedical Engineering
University of Pavia
Pavia, Italy

Anita Bertoni
Dept. of Electrical, Computer and Biomedical Engineering
University of Pavia
Pavia, Italy

Alessandro Ramalli
Dept. of Cardiovascular Sciences
KU Leuven
Leuven, Belgium

Alessandro S. Savoia
Dept. of Engineering
Roma Tre University
Rome, Italy

Giovanni Magenes
Dept. of Electrical, Computer and Biomedical Engineering
University of Pavia
Pavia, Italy

***Abstract*—In quasi-static elastography, the operator compresses the tissue under exam with the probe, while the scanner processes the beamformed frames, by means of correlation or signal phase analysis techniques, to estimate both the displacement and the strain. However, the quality of estimates may be influenced by the speckle quality and hence by the implemented beamforming algorithm. Therefore, in this work we investigate the effects of coherence-based beamforming techniques, providing better images than conventional Delay and Sum (DAS), on the estimation of axial/lateral displacement and strain in quasi-static elastography of the breast. Simulations were used to evaluate the error on axial and lateral displacement estimations obtained by 2D normalized cross-correlation (2D-NCC) with polynomial fitting, as compared to the ground truth given by finite-element modeling. Experimental breast phantom acquisitions where instead evaluated in terms of elastographic contrast-to-noise-ratio (CNRe) and non-uniformity (NU) level. Results show that similar performance in axial displacement estimation is achieved by 2D-NCC with all beamformers, while using coherence beamforming provides more accurate estimates of lateral displacement. However, the analysis of CNRe and NU in experimental axial/lateral strain images does not show any significant improvement as compared to DAS when any of these beamformers is employed.**

Keywords—breast imaging, beamforming, coherence factor, displacement estimation, filtered delay multiply and sum, phase coherence, quasi-static ultrasound elastography, sign coherence

I. Introduction

Elastography performs a remote palpation of internal organs to assess their mechanical properties [1]. In particular, the so-called quasi-static elastography [2] relies on the application of a gentle compression of the tissues under exam through the probe, and on the estimation of the displacement/strain that these tissues undergo. This strain, even if only indirectly, can be related to the elasticity modulus of the tissue, thus providing a qualitative map of stiffness. The elastogram is usually superimposed to the B-mode image and is represented as a color-coded image, where soft tissues appear as red areas and hard structures as blue regions. This technique can be applied, for example, to assess the stiffness of breast, as tumors are generally harder than the surrounding tissues [3].

In breast elastography, usually, only axial strain is computed through the application of 1D displacement estimation techniques, e.g. based on cross-correlation or zero phase estimation. On the other hand, however, it is known that biological tissues are almost incompressible, thus an axial compression is likely to cause an expansion of tissues in the lateral direction too [4], i.e. in the direction perpendicular to the ultrasound beam axis and parallel to the surface of the array. Actually, this could provide additional diagnostic information; it should be considered, as an example, that in cardiac applications the heart strain has to be evaluated in 3D, or that, thanks to lateral strain, shear strain and Poisson's ratio can be used to estimate tumors mobility, which provides further indications on their malignancy [4]. However, lateral displacement/strain estimation is a complex task, because of the reduced spatial sampling of signals (which is limited by the array pitch) and the lack of phase information in that direction. For this reason, methods for axial/lateral displacement computation are mainly based on 2D normalized cross-correlation (2D-NCC) algorithms [5], with additional interpolation or correlation-peak fitting procedures to achieve sub-sample accuracy [6].

Displacement estimation techniques for the reconstruction of elastograms in quasi-static elastography are applied on radiofrequency (RF) images, i.e. on the RF image scan lines obtained after beamforming in reception. Generally, standard Delay and Sum (DAS) beamforming is applied; however, higher performance beamformers have been proposed up to now, which are able to improve image contrast and lateral resolution [7], but slightly compromising the speckle pattern uniformity.

Therefore, in this paper we aim to investigate whether starting from an RF image obtained by applying a coherence-based beamforming method can lead to an improved estimation of displacement in elastography images. Particularly, we focus

This work was partially supported by the University of Pavia under the Blue Sky Research project MULTIWAVE. A. Ramalli was supported by the European Union's Horizon 2020 research and innovation programme under the Marie Skłodowska-Curie grant agreement No 786027 (ACOUSTIC project).

on Coherence Factor (CF) [8], Generalized CF (GCF) [9], Phase and Sign CF (PCF, SCF) [10], and Filtered Delay Multiply and Sum (FDMAS) [7] beamforming, which have shown excellent performance in B-mode imaging as compared to DAS. A 2D-NCC procedure with polynomial fitting is applied to simulated RF images obtained with these beamforming techniques, and the error on estimated displacement is then evaluated. Finally, their performance is also investigated in terms of image quality (i.e. contrast and uniformity) on experimental breast phantom elastograms.

II. Materials and Methods

A. Coherence-Based Beamforming Algorithms

- Coherence Factor

The CF [8] provides a measure of the quality of focusing and is computed dividing the coherent sum of received (and delayed) RF signals $s_n(t)$ by their incoherent sum, obtaining a number that ranges from 0 to 1. If N is the number of elements in the active aperture, then the beamformed output signal $y_{cf}(t)$ is obtained by computing the CF for each time sample and using it to weight the DAS signal $y_{das}(t)$, as follows:

$$y_{cf}(t) = y_{das}(t) \cdot CF(t) = y_{das}(t) \cdot \frac{\left|\sum_{n=1}^{N} s_n(t)\right|^2}{N\sum_{n=1}^{N}|s_n(t)|^2}. \quad (1)$$

- Generalized Coherence Factor

GCF [9] is computed as the ratio between the energy of RF signals at frequencies lower than a certain cutoff level (M_0), and the total energy. The GCF-weighted RF lines are obtained as:

$$y_{gcf}(t) = y_{das}(t) \cdot GCF(t) = y_{das}(t) \cdot \frac{\sum_{k=0}^{M_0} |S(k,t)|^2}{\sum_{k=0}^{N-1} |S(k,t)|^2} \quad (2)$$

where $S(k, t)$ is the spectrum of $s_n(t)$ and k represents the spatial frequency index. GCF is equivalent to CF when M_0=0.

- Phase and Sign Coherence Factors

In the PC algorithm case, the coherence of received signals after focusing is evaluated by analyzing the distribution of their instantaneous phases $\varphi_n(t)$, particularly their standard deviation $\sigma(\varphi_n(t))$. The PC factor (PCF), which is again a value in the [0; 1] range, is computed as [10]:

$$PCF(t) = \max\left\{0, 1 - \frac{\gamma}{\pi/\sqrt{3}}\sigma(\varphi_n(t))\right\} \quad (3)$$

where γ is a user-defined parameter in the range [0; 1] used to tune PCF sensitivity and off-axis signal rejection. SCF is instead computed considering the standard deviation of signs $b_n(t)$ of RF signal samples:

$$SCF(t) = \left|1 - \sigma(b_n(t))\right|^q \quad (4)$$

where $q \geq 0$ is again a parameter used to tune SCF sensitivity. The beamformed signal is finally obtained by multiplying PCF or SCF by the DAS output, as for CF weighting.

- Filtered Delay Multiply and Sum

The FDMAS algorithm [7] consists in rescaling the RF signal amplitudes by means of a signed square root, then coupling, multiplying and finally summing them up:

$$y_{fdmas}(t) = \sum_{n=1}^{N-1}\sum_{m=n+1}^{N} sign(s_n(t)s_m(t)) \cdot \sqrt{|s_n(t)s_m(t)|}\,. \quad (5)$$

The output of eq. (5) is band-pass filtered around the second harmonic component that originates after these non-linear operations, which basically correspond to the computation of the receive aperture spatial autocorrelation.

B. Displacement Estimation with 2D Cross-Correlation

Displacement estimation is based on the computation of 2D-NCC (R) between 2D kernels on the pre- and post-compression RF image frames. Windows are generally overlapped and are moved until the whole image space is covered. The window over the post-compression image is shifted step by step along the lateral direction, while axially it is moved adaptively based on the axial displacement estimated at the previous step.

At each step, $R(z, x)$ is computed as [5]:

$$R(z,x) = \frac{\sum_{i=z}^{z+W_z-1}\sum_{j=x}^{x+W_x-1} y_1(i,j) \cdot y_2(i+\tau, j+\delta)}{\sqrt{\sum_{i=z}^{z+W_z-1}\sum_{j=x}^{x+W_x-1} y_1^2(i,j) \cdot \sum_{i=z}^{z+W_z-1}\sum_{j=x}^{x+W_x-1} y_2^2(i+\tau, j+\delta)}} \quad (6)$$

where y_1 and y_2 are the RF image lines in the pre- and post-compression frames, respectively; W_z and W_x are the kernel size along axial and lateral direction respectively, while τ and δ represent the NCC lags (in samples). The 2D-NCC peak position provides an estimate of the spatio-temporal shift that exists between the pre- and post-compression kernels, and can be stored to generate a map of axial and lateral displacement. These are in the end converted into axial and lateral strain maps (elastograms), respectively, by computing the gradient of displacement (along z for axial displacement, and along x for lateral displacement).

For a more accurate estimation of sub-sample lateral displacement, a polynomial fitting procedure of 2D-NCC can be applied; different types of fitting curves have been proposed in the literature (e.g. parabolic, cubic spline, etc. [6]). In this work a quartic spline polynomial was fitted to the peak of R and to its 24 neighboring lags in 2D.

C. Simulation and Experimental Setup

Simulations were performed using Finite Element Method (FEM) to simulate tissue compression, and Field II [11], [12] for RF signals generation. A 30×30 mm elasticity phantom (background shear modulus = 10 kPa) with a spherical, stiffer (60 kPa), isoechoic, 6-mm target was modeled using ANSYS (ANSYS Inc., Canonsburg, PA, USA). An external load was applied on its top surface to simulate a maximum displacement of 0.5 mm axially (z axis) and of 0.3 mm laterally (x axis). The FEM model node positions were resampled to derive a random distribution of scatterers, with more than 10 scatterers per resolution cell, as required for a correct speckle formation. This procedure was applied both to the reference FEM model and to

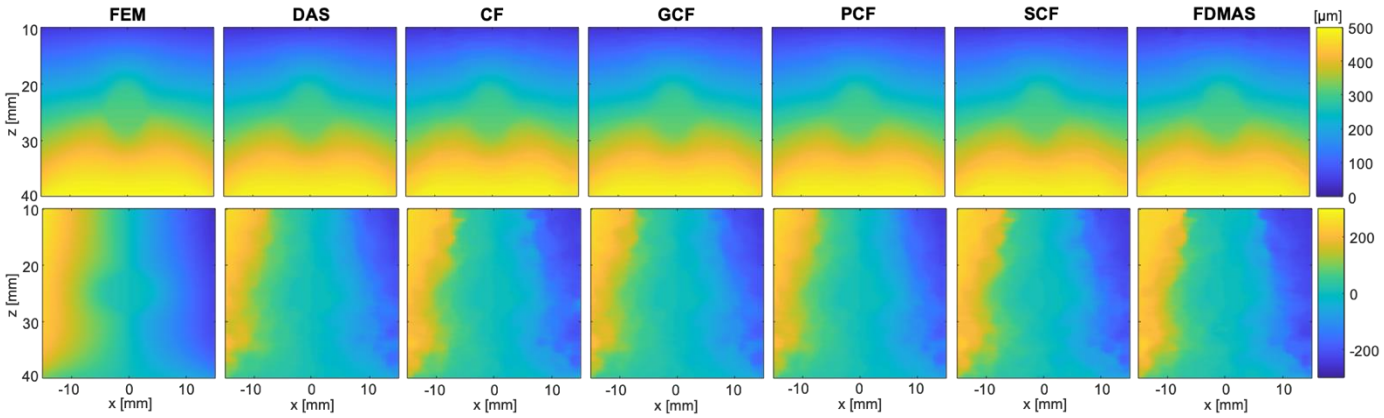

Fig. 1. Axial (top row) and lateral (bottom row) displacement maps obtained from FEM simulations (reference) and with 2D-NCC combined with different beamforming methods.

the one obtained after the load application. The pre- and post-compression numerical phantoms were thus imported in MATLAB for ultrasound imaging simulations with Field II. A 5 MHz linear array was modeled (192 elements, pitch=0.245 mm, 64-element active aperture) to simulate the scan of 192 RF lines. The focal depth in transmission was set to 25 mm, while dynamic focusing was applied in reception. The sampling frequency was 100 MHz.

The ULA-OP scanner [13] was used for experimental acquisitions at 26 fps on a CIRS breast phantom (model 059, CIRS Inc., Norfolk, VA) with inclusions about 2 times harder than the background, which has a ~20 kPa elastic modulus. The LA533 linear-array probe by Esaote (Esaote S.p.A, Florence, Italy) was used to acquire 192 RF lines at 7 MHz, focusing at 20 mm depth. Signals sampled at 50 MHz were then imported in MATLAB for processing.

The RF frames were reconstructed with DAS, CF, GCF (M_0=2), PCF (γ=0.6), SCF (γ=0.6) and FDMAS beamforming. Elastograms were finally obtained with 2D-NCC applied to consecutive frame couples, considering a 140×10 samples ($z \times x$) kernel with Hann tapering along the z direction, and finally filtered by a 2×2 mm median filter. On simulated data, the performance of the algorithms was quantitatively evaluated by computing the Root Mean Squared Error (RMSE) and median error (mE) on displacement images as compared to the reference FEM ones. In the experimental case, instead, due to the lack of a reference displacement map, elastogram image quality was quantified in terms of elastographic contrast-to-noise ratio (CNRe) and non-uniformity level (NU) [14].

III. Results

Results of simulations are shown in Fig. 1, where the reference axial/lateral displacements obtained from FEM and the ones estimated with 2D-NCC starting from differently beamformed RF images are presented. As it can be seen, estimates are in all cases similar to FEM results, but some errors are present, especially for lateral displacement.

In Table I, the RMSE and mE values obtained for all images are provided. RMSE values are generally higher than mE ones, due to the presence of several outlier errors that often appear in the displacement estimates. For axial displacement, error values obtained for all beamformers are similar. In the lateral case instead, some more significant differences exist; in particular, with CF, SCF and FDMAS, a RMSE which is from 2.4 μm (PCF) to 5.5 μm (SCF) lower than DAS (RMSE=29.3 μm) is obtained. Percentage differences on RMSE and mE vs. DAS are shown in Table II: negative values indicate that lower errors are achieved. The table shows that improvements are achieved by coherence-based beamformers in almost all cases; such improvements are generally low in the axial case and increase in the lateral one. CF, SCF and FDMAS show the most significant differences from DAS on lateral displacement estimation, achieving an up to ~32% improvement with SCF.

In Fig. 2, one elastography frame is shown (both axial and lateral strain are represented) for experimental acquisitions on the breast phantom. The measured CNRe and NU values are reported in Table III. Results show that all axial elastograms look very similar, as well as their NU, except the FDMAS one which has some overestimated areas on the target borders and the lowest CNRe. With all coherence-based beamformers, CNRe is lower than the DAS one, especially with CF, SCF and FDMAS. Lateral elastograms present some more significant differences, as the target shape looks qualitatively more defined

TABLE I. RMSE and mE on Axial/Lateral Displacement Estimates

	Error [μm]	Beamformer					
		DAS	***CF***	***GCF***	***PCF***	***SCF***	***FDMAS***
AD	RMSE	9.51	9.16	9.48	9.56	9.67	9.41
AD	mE	8.85	8.37	8.81	8.87	8.92	8.67
LD	RMSE	29.3	25.5	29.3	26.9	23.8	26.1
LD	mE	25.3	18.8	25	22.3	17.2	18

AD = Axial Displacement image, LD = Lateral Displacement image.

TABLE II. Percentage Error on Displacement Estimation vs. DAS

	% error	Beamformer				
		CF	***GCF***	***PCF***	***SCF***	***FDMAS***
AD	RMSE	-3.7%	-0.4%	+0.4%	+1.6%	-1.1%
AD	mE	-5.5%	-0.5%	+0.2%	+0.8%	-2%
LD	RMSE	-13.1%	-0.1%	-8.1%	-18.7%	-10.8%
LD	mE	-25.7%	-1.4%	-9.3%	-32.2%	-28.9%

AD = Axial Displacement image, LD = Lateral Displacement image.

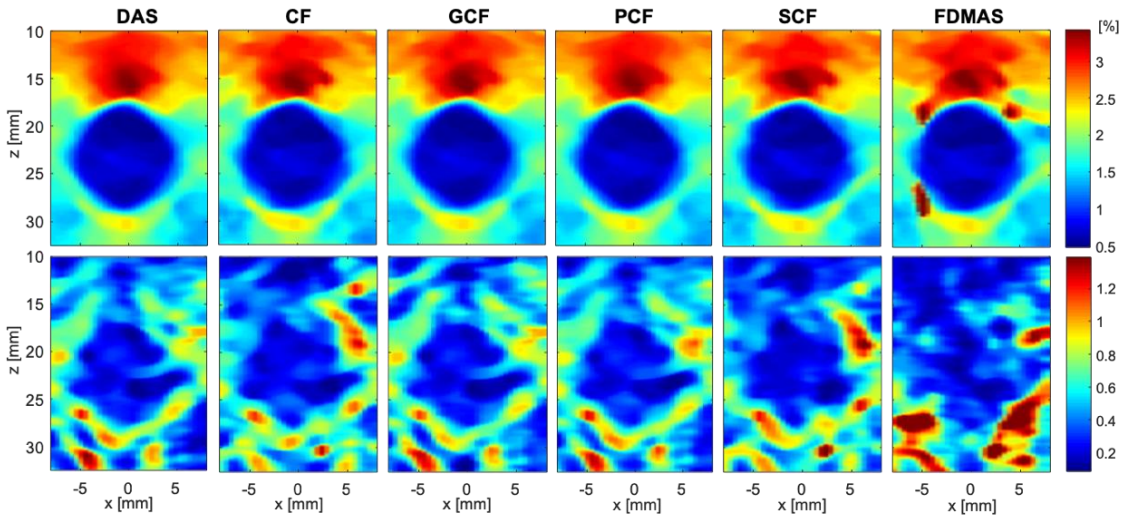

Fig.2. Axial (top row) and lateral (bottom row) strain images of the breast phantom, obtained with different beamformers and 2D-NCC.

TABLE III. CNRe AND NU OF BREAST PHANTOM ELASTOGRAMS

	Param	Beamformer					
		DAS	***CF***	***GCF***	***PCF***	***SCF***	***FDMAS***
AS	CNRe	20.3	17.8	19.6	19.8	16.9	12.5
AS	NU	10.6%	11.1%	10.9%	10.4%	12.2%	12.5%
LS	CNRe	1.2	0.8	1.2	1	0.6	0.3
LS	NU	41.6%	41%	41.8%	40.1%	45.6%	45%

AS = Axial Strain image, LS = Lateral Strain image.

with CF and SCF. GCF and PCF behave similarly to DAS, while FDMAS gives the noisiest output. However, since images also look sharper, CNRe is lower with CF, PCF, SCF and FDMAS than with DAS. Also NU is about 4% worse with SCF and FDMAS than with DAS.

IV. DISCUSSION AND CONCLUSION

2D-NCC with polynomial fitting allows estimating both axial and lateral displacement for the reconstruction of breast elastograms in both directions. However, lateral displacement/strain images show a lower accuracy and quality than axial ones, since estimation in this direction suffers from several limitations, as explained previously.

In this paper we investigated whether applying coherence-based beamforming followed by 2D-NCC could lead to more accurate displacement estimates and elastograms with higher contrast/uniformity than DAS. Our simulation results show that an improvement can be achieved in the estimation of lateral displacement if coherence-based beamformers are applied, particularly with CF, SCF and FDMAS, while performance on axial displacement is similar to that of DAS. Axial strain quality is similar in all cases too, while for lateral strain sharper images are obtained with these beamformers, where the target seems better defined. However, CNRe and NU are lower than those of DAS. In particular, FDMAS gives the worst results, but probably in this case a different window size should be chosen, due to the doubled frequency. Further analyses are thus foreseen to investigate more in depth the effects of coherence-based beamformers on lateral elastograms.

REFERENCES

[1] J.-L. Gennisson, T. Deffieux, M. Fink, M. Tanter, "Ultrasound elastography: Principles and techniques," *Diagn. Interv. Imaging*, vol. 94, pp. 487-495, 2013

[2] J. Ophir, E. I. Cespedes H. Ponnekanti, Y. Yazdi, X. Li, "Elastography: a method for imaging the elasticity in biological tissues," *Ultrason. Imaging*, vol. 13, pp. 111-134, 1991.

[3] A. Thitaikumar, l. M. Mobbs, C. M. Kraemer-Chant, B. S. Garra, and J. Ophir, "Breast tumor classification using axial shear strain elastography: a feasibility study," *Phys. Med. Biol*., vol. 53, no. 7, pp. 4809–4823, 2008.

[4] J. Luo, and E. E. Konofagou, "Effects of Various Parameters on Lateral Displacement Estimation in Ultrasound Elastography", *Ultrasound. Med. Biol.*, vol. 35, no. 8, pp. 1352–1366, 2009.

[5] J. Luo, and E. E. Konofagou, "A Fast Normalized Cross-Correlation Calculation Method for Motion Estimation," *IEEE Trans. Ultrason,. Ferroelectr., Freq. Control*, vol. 57, no. 6, pp. 1347–1357, 2010.

[6] R. Z. Azar, O. Goksel, S. E. Salcudean, "Sub-Sample Displacement Estimation From Digitized Ultrasound RF Signals Using Multi-Dimensional Polynomial Fitting of the Cross-Correlation Function," *IEEE Trans. Ultrason., Ferroelectr., Freq. Control*, vol. 57, no. 11, pp. 2403– 2420, 2010.

[7] G. Matrone, A. S. Savoia, G. Caliano, G. Magenes, "The Delay Multiply and Sum beamforming algorithm in ultrasound B-mode medical imaging," *IEEE Trans. Med. Imag.*, vol. 34, no. 4, pp. 940-949, 2015.

[8] K. W. Hollmand, K. W. Rigby, and M. O'donnell, "Coherence factor of speckle from a multi-row probe," in *Proc. IEEE Int. Ultrasonics Symp*., 1999, pp. 1257–1260.

[9] P.-C. Li and M.-L. Li, "Adaptive imaging using the generalized coherence factor," *IEEE Trans. Ultrason., Ferroelectr., Freq. Control*, vol. 50, no. 2, pp. 128–142, 2003.

[10] J. Camacho, M. Parrilla, C. Fritsch, "Phase coherence imaging," *IEEE Trans. Ultrason., Ferroelectr., Freq. Control*, vol. 56, no. 5, pp. 958-974, 2009.

[11] J. A. Jensen, N. B. Svendsen, "Calculation of pressure fields from arbitrarily shaped, apodized, and excited ultrasound transducers," *IEEE Trans. Ultrason., Ferroelectr., Freq. Control*, vol. 39, no. 2, pp. 262-267, 1992.

[12] J. A. Jensen, "Field: a program for simulating ultrasound systems," *Med. Biol. Eng. Comput.*, vol. 34, pp. 351-353, 1996.

[13] E. Boni, L. Bassi, A. Dallai, F. Guidi, A. Ramalli, S. Ricci, R. J. Housden, and P. Tortoli, "A reconfigurable and programmable FPGA-based system for nonstandard ultrasound methods," *IEEE Trans. Ultrason. Ferroelectr. Freq. Control*, vol. 59, no. 7, pp. 1378–1385, 2012.

[14] A. Ramalli, O. Basset, C. Cachard, E. Boni, P. Tortoli, "Frequency-domain-based strain estimation and high-frame-rate imaging for quasi-static elastography," *IEEE Trans. Ultrason. Ferroelectr. Freq. Control*, vol. 59, no. 4, pp. 817-824, 2012